Spin Hall and spin Nernst effects in graphene with intrinsic and Rashba spin–orbit interactions*

Zhu Guo-Bao(朱国宝)†

Beijing National Laboratory for Condensed Matter Physics, Institute of Physics, Chinese Academy of Sciences, Beijing 100190, *China*

(Received 30 March 2012; revised manuscript received 4 June 2012)

The spin Hall and spin Nernst effects in graphene are studied based on Green's function formalism. We calculate intrinsic contributions to spin Hall and spin Nernst conductivities in the Kane–Mele model with various structures. When both intrinsic and Rashba spin–orbit interactions are present, their interplay leads to some characteristics of the dependence of spin Hall and spin Nernst conductivities on the Fermi level. When the Rashba spin–orbit interaction is smaller than intrinsic spin–orbit coupling, a weak kink in the conductance appears. The kink disappears and a divergence appears when the Rashba spin–orbit interaction enhances. When the Rashba spin–orbit interaction approaches and is stronger than intrinsic spin–orbit coupling, the divergence becomes more obvious.

Keywords: graphene, spin–orbit interaction, Green's function theory

PACS: 73.43.–f, 73.20.Hb, 73.61.Wp **DOI:** 10.1088/1674-1056/21/11/117309

1. Introduction

Recently, the spin Hall effect (SHE) has become one of the most exciting subjects in spintronics and has been studied both experimentally and theoretically,[1−6] given that it offers a possibility of controlling the electron spin in spintronics applications. In the spin Hall effect, a transverse current which comes from the transverse motion of two kinds of spin in opposite directions, is induced by a longitudinal electric field. Generally, the SHE is associated with either an intrinsic or extrinsic mechanism, depending on the origin of the SHE. The intrinsic SHE which does not require the presence of impurities, may be described in terms of the Berry phase formalism,[7,8] and also referred to as the topological SHE. While the corresponding extrinsic mechanism is related to the impurity scattering (side jump and skew scattering).

A driving power or voltage may be generated not only by an electric field, but also due to a temperature gradient. One of the most important examples is the Seebeck effect.[9,10] Motivated by the development of spintronics, the spin Seebeck effect has become an important subject of current research, where the longitudinal spin current and spin voltage are generated by the temperature gradient. Therefore, it is reasonable to believe that the temperature gradient may lead to anomalous spin Nernst effects[11] in systems with a spin–orbit interaction.

In this paper, we study the spin Hall conductivity (SHC) and spin Nernst conductivity (SNC) in graphene with intrinsic and extrinsic spin–orbit interactions. Since the discovery in an experiment in 2004,[12] graphene has been one of the most interesting and widely-studied materials and has paved the way for the development of carbon-based spintronics. Graphene is a two-dimensional allotrope of carbon with a honeycomb structure, and a linear dispersion relationship in momentum at low-energy scales. The quasiparticle can be described in terms of Dirac fermions. The relativistic nature of the quasiparticle in graphene leads to unusual transport properties. The Kane–Mele model[13,14] is an idealized model of graphene with intrinsic and extrinsic spin–orbit interactions, and many authors have pointed out that the SHE can occur in graphene with an intrinsic spin–orbit interaction. Unfortunately the intrinsic spin–orbit interaction is so weak that it is difficult to realize in experiments so far. Furthermore, the Rashba spin–orbit interaction is also weak. However, recent experiments have suggested that the Rashba spin–orbit interaction can be very strong for the graphene grown on a substrate.[15,16] The Rashba spin–orbit interaction

*Project supported by the National Natural Science Foundation of China (Grant No. 10934010) and the National Basic Research Program of China (Grant Nos. 2011CB921502 and 2012CB821305).

†Corresponding author. E-mail: zhuguobao@gmail.com

© 2012 Chinese Physical Society and IOP Publishing Ltd

can also be controlled via the impurity coverage.[17] Therefore, we aim to study the interesting physics of the interplay of the two types of spin–orbit interactions in SHC and SNC.

The paper is organized as follows. In Section 2, we describe the Kane–Mele model in graphene and present a general formulae for SHC and SNC. In Section 3, the SHC and SNC in graphene with various structures are described. Conclusions are given in Section 4.

2. Model and general formula for spin Hall conductivity

2.1. Kane–Mele model

The effective Hamiltonian[14] of graphene in the presence of spin–orbit interactions is expressed as

$$H = H_0 + H_\Delta + H_\mathrm{R}, \tag{1}$$

The first term, H_0, describes the low-energy electronic states around the Dirac points K and K' in the Brillouin zone, and has the form

$$H_0 = \hbar v_\mathrm{F}(p_x\boldsymbol{\sigma}_x\boldsymbol{\tau}_z + p_y\boldsymbol{\sigma}_y). \tag{2}$$

This term comes from the nearest-neighbour-hopping term in the tight-binding approximation. The $\boldsymbol{\sigma} = (\boldsymbol{\sigma}_x, \boldsymbol{\sigma}_y, \boldsymbol{\sigma}_z)$ and $\boldsymbol{\sigma}_0$ stand for the Pauli matrices which act on pseudospin space. The Pauli matrices $\boldsymbol{\tau} = (\boldsymbol{\tau}_x, \boldsymbol{\tau}_y, \boldsymbol{\tau}_z)$ and $\boldsymbol{\tau}_0$ act on the two valley space. The v_F denotes the electron's Fermi velocity. For simplicity, we take $\hbar = v_\mathrm{F} = 1$ throughout the paper. The second term is the intrinsic spin–orbit interaction induced by the atomic potentials or topological term and takes the following form:

$$H_\Delta = -\Delta\boldsymbol{\sigma}_z\boldsymbol{s}_z\boldsymbol{\tau}_z, \tag{3}$$

which is opposite to the original papers.[18,19] The Pauli matrices $\boldsymbol{s} = (\boldsymbol{s}_x, \boldsymbol{s}_y, \boldsymbol{s}_z)$ and $\boldsymbol{s}_0$ act on the real spin space. Throughout this paper, I assume that $\Delta > 0$. The last term

$$H_\mathrm{R} = -\frac{\lambda_\mathrm{R}}{2}(\boldsymbol{\sigma}_x\boldsymbol{s}_y\boldsymbol{\tau}_z - \boldsymbol{\sigma}_y\boldsymbol{s}_x) \tag{4}$$

is the Hamiltonian of Rashba spin–orbit interaction, where λ_R is the corresponding coupling parameter.

The eigenvalues of the Hamiltonian are given by

$$E(\sigma, s, p) = \sigma\sqrt{p^2 + (\Delta + s\lambda_\mathrm{R}/2)^2} + s\lambda_\mathrm{R}/2, \tag{5}$$

where $\sigma = \pm$ refer to the conduction and valence bands, and $s = \pm 1$ correspond to the spin-up and spin-down electrons, respectively. The corresponding chiral base wave functions take the following forms:[18]

$$|+, s\rangle = \frac{1}{\sqrt{2}}\left[\mathrm{e}^{\mathrm{i}\phi}\sin\frac{\theta_s}{2}, \cos\frac{\theta_s}{2}, s\mathrm{i}\cos\frac{\theta_s}{2}, s\mathrm{i}\mathrm{e}^{-\mathrm{i}\phi}\sin\frac{\theta_s}{2}\right]^\mathrm{T}, \tag{6}$$

$$|-, s\rangle = \frac{1}{\sqrt{2}}\left[\mathrm{e}^{\mathrm{i}\phi}\cos\frac{\theta_s}{2}, -\sin\frac{\theta_s}{2}, -s\mathrm{i}\sin\frac{\theta_s}{2}, s\mathrm{i}\mathrm{e}^{-\mathrm{i}\phi}\cos\frac{\theta_s}{2}\right]^\mathrm{T}, \tag{7}$$

where superscript T denotes the transpose of the matrix, $\cos\theta_\pm = (\Delta \pm \lambda_\mathrm{R}/2)/[\sqrt{p^2 + (\Delta \pm \lambda_\mathrm{R}/2)^2}]^{1/2}$ and $\cos\phi = p_x/p$. When the Rashba coupling vanishes, the intrinsic spin–orbit interaction opens up a gap which breaks the energy spectrum into an electron band at positive energies and a hole band at negative energies. When only the Rashba spin–orbit interaction is present, the Rashba spin–orbit interaction breaks the spin degeneracy. When both intrinsic and Rashba spin–orbit interactions are present, their interplay leads to different dispersion relations. When λ_R reaches a critical value 2Δ, the band gap closes. For the case of $\Delta > \lambda_\mathrm{R}/2$ (see Fig. 1(a)), the system is gaped, and two valence bands are degenerate only at $p = 0$. When $\Delta = \lambda_\mathrm{R}/2$ (see Fig. 1(b)), the dispersions are threefold degenerate at $p = 0$. For $\Delta < \lambda_\mathrm{R}/2$ (see Fig. 1(c)), one conduction band and one valence band are degenerate at $p = 0$.

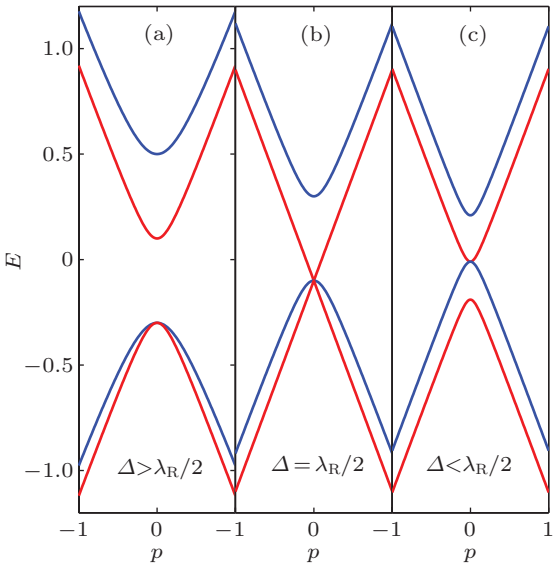


Fig. 1. (colour online) Dependence of the energy spectrum on the type of spin–orbit interactions. The blue and red curves denote the energy spectra with different spins. (a) $\Delta > \lambda_\mathrm{R}/2$, (b) $\Delta = \lambda_\mathrm{R}/2$, and (c) $\Delta < \lambda_\mathrm{R}/2$.

2.2. Green's function for the SHC and SNC

Based on Green's function theory,[20−23] the spin hall conductivity in a perfect crystal lattice, for a z-component spin current flowing in the x direction under an electric field along the y direction ($\boldsymbol{E} = (0, E, 0)$), can be expressed as

$$\sigma^s_{xy} = \sigma^{s1}_{xy} + \sigma^{s2}_{xy}. \tag{8}$$

The first term on the right of Eq. (8) is the contribution from the Fermi surface, the other term is the contribution from the Fermi sea, and

$$\begin{aligned}\sigma^{s1}_{xy} = &-\frac{e\hbar}{2}\int\frac{\mathrm{d}\varepsilon}{2\pi}\partial_\varepsilon f(\varepsilon)\int\frac{\mathrm{d}^2p}{(2\pi\hbar)^2}\mathrm{Tr}\Big[\hat{j_s}(p)G^{\mathrm{R}}_0(\varepsilon,p)\hat{v}_y(p)(G^{\mathrm{A}}_0(\varepsilon,p)-G^{\mathrm{R}}_0(\varepsilon,p))\\ &-\hat{j_s}(p)(G^{\mathrm{A}}_0(\varepsilon,p)-G^{\mathrm{R}}_0(\varepsilon,p))\hat{v}_y(p)G^{\mathrm{R}}_0(\varepsilon,p)\Big],\end{aligned} \tag{9}$$

$$\begin{aligned}\sigma^{s2}_{xy} = &-\frac{e\hbar}{2}\int\frac{\mathrm{d}\varepsilon}{2\pi}f(\varepsilon)\int\frac{\mathrm{d}^2p}{(2\pi\hbar)^2}\mathrm{Tr}\Big[\hat{j_s}(p)G^{\mathrm{A}}_0(\varepsilon,p)G^{\mathrm{A}}_0(\varepsilon,p)\hat{v}_y(p)G^{\mathrm{A}}_0(\varepsilon,p)\\ &-\hat{j_s}(p)G^{\mathrm{A}}_0(\varepsilon,p)\hat{v}_y(p)G^{\mathrm{A}}_0(\varepsilon,p)G^{\mathrm{A}}_0(\varepsilon,p)-(G^{\mathrm{A}}_0\to G^{\mathrm{R}}_0)\Big],\end{aligned} \tag{10}$$

where $f(\varepsilon)$ is the Fermi distribution, $\hat{j_s} = \{\hat{v}_x, \hat{s}_z\}/2$ is the spin current density operator, $\hat{v}_{x,y} = (1/\hbar)(\partial H/\partial p_{x,y})$ is the velocity operator, and

$$G^{\mathrm{R,A}}_0(\varepsilon,p) = [\varepsilon - H_0(p) \pm \mathrm{i}0^+]^{-1} \tag{11}$$

is the retarded (advanced) Green's function in the clean limit.

In the low-temperature regime, according to the Mott rule,[21,24] the SNC can be written as follows:

$$\alpha^s_{xy} = \frac{\pi^2k^2_{\mathrm{B}}}{3e}T\left[\frac{\mathrm{d}}{\mathrm{d}\varepsilon}\sigma^s_{xy}(\varepsilon)\right]_{\varepsilon=\mu}, \tag{12}$$

where T stands for temperature, μ is the Fermi energy, and k_{B} is the Boltzman constant.

3. Spin Hall and spin Nernst conductivity

In this section, I give the analytical expressions of intrinsic contributions to the SHC and SNC. Based on Eq. (9) and (10), I obtain the intrinsic contribution by using the residue theorem as

$$\begin{aligned}\sigma^s_{xy} = &\, e\hbar\int\frac{\mathrm{d}^2p}{(2\pi\hbar)^2}\mathrm{Im}\sum_{\sigma_1,\sigma_2,s_1,s_2}\frac{f(E(\sigma_1,s_1))-f(E(\sigma_2,s_2))}{[E(\sigma_1,s_1)-E(\sigma_2,s_2)]^2}\\ &\times\langle\sigma_1,s_1|\hat{j_s}|\sigma_2,s_2\rangle\langle\sigma_2,s_2|\hat{v}_y|\sigma_1,s_1\rangle.\end{aligned} \tag{13}$$

Using Eq. (12), the corresponding SNC in the low-temperature regime is given by

$$\begin{aligned}\alpha^s_{xy} = &\,\frac{2\pi^2k^2_{\mathrm{B}}\hbar}{3}T\int\frac{\mathrm{d}^2\boldsymbol{p}}{(2\pi\hbar)^2}\mathrm{Im}\sum_{\sigma_1,\sigma_2,s_1,s_2}\frac{\delta(\mu-E(\sigma_1,s_1))}{[E(\sigma_1,s_1)-E(\sigma_2,s_2)]^2}\\ &\times\langle\sigma_1,s_1|\hat{j_s}|\sigma_2,s_2\rangle\langle\sigma_2,s_2|\hat{v}_y|\sigma_1,s_1\rangle.\end{aligned} \tag{14}$$

These contributions are only dependent on the band structure of the Kane–Mele model. In the eigenstate representation (Eqs. (6) and (7)), the SHC and SNC are determined by the off diagonal matrix elements of the spin density operator and velocity operator. When the Rashba coupling vanishes, one can obtain

$$\sigma^s_{xy} = \frac{\Delta}{|\mu|}\frac{e}{2\pi}, \tag{15}$$

$$\alpha^s_{xy} = -\frac{|\mu|\Delta}{\mu^3}\frac{\pi k^2_{\mathrm{B}}T}{6}, \tag{16}$$

for $|\mu| > \Delta$, and $\sigma_{xy} = e/2\pi$, $\alpha_{xy} = 0$ for $|\mu| < \Delta$. They are consistent with the results obtained in previous work.[14,25]

When both intrinsic and Rasha spin–orbit interactions are present in the system, there are four regimes for the position of the Fermi energy (μ): (i) $\mu > \Delta + \lambda_{\mathrm{R}}$, (ii) $|\Delta - \lambda_{\mathrm{R}}/2| - \lambda_{\mathrm{R}}/2 < \mu < \Delta + \lambda_{\mathrm{R}}$,

(iii) $-|\Delta-\lambda_{\rm R}/2|-\lambda_{\rm R}/2<\mu<|\Delta-\lambda_{\rm R}/2|-\lambda_{\rm R}/2$, and (iv) $\mu<-|\Delta-\lambda_{\rm R}/2|-\lambda_{\rm R}/2$. From Eqs. (13) and (14), in the region (i), I obtain

$$\sigma^s_{xy} = \left[\frac{\mu(\mu+\Delta)}{\mu^2-\lambda_{\rm R}^2/4} - 2\eta\Delta/\lambda_{\rm R}\log\frac{2\Delta+\lambda_{\rm R}}{|2\Delta-\lambda_{\rm R}|}\right]\frac{e}{4\pi}, \quad (17)$$

$$\alpha^s_{xy} = -\frac{2\Delta(\mu^2+\lambda_{\rm R}^2/4)+\mu\lambda_{\rm R}^2}{(\mu^2-\lambda_{\rm R}^2/4)^2}\frac{\pi k_{\rm B}^2T}{24}, \quad (18)$$

where $\eta=1-\delta(2\Delta-\lambda_{\rm R})$. In the region (ii), I obtain

$$\sigma^s_{xy} = \left[\frac{\mu}{\lambda_{\rm R}}-\mu(\Delta-\frac{\lambda_{\rm R}}{2})/\lambda_{\rm R}(\mu+\lambda_{\rm R}/2) - \frac{2\Delta}{\lambda_{\rm R}}\log\frac{\mu+\Delta}{|2\Delta-(-1)^{\eta+1}\lambda_{\rm R}|}\right]\frac{e}{4\pi}, \quad (19)$$

$$\alpha^s_{xy} = \left[\frac{1}{\lambda_{\rm R}}-\frac{\Delta-\lambda_{\rm R}/2}{2(\mu+\lambda_{\rm R}/2)^2} - \frac{2\Delta}{\lambda_{\rm R}}\frac{1}{\mu+\Delta}\right]\frac{\pi k_{\rm B}^2T}{12}. \quad (20)$$

For the region (iii), I obtain

$$\sigma^s_{xy} = \left[\frac{\mu}{\lambda_{\rm R}}-\frac{\mu(\Delta+\lambda_{\rm R}/2)}{\lambda_{\rm R}(\mu-\lambda_{\rm R}/2)} - \frac{2\Delta}{\lambda_{\rm R}}\log\frac{\mu+\Delta}{|2\Delta-\lambda_{\rm R}|}\right]\theta(\lambda_{\rm R}-2\Delta)\frac{e}{4\pi}, \quad (21)$$

$$\alpha^s_{xy} = \left[\frac{1}{\lambda_{\rm R}}+\frac{\Delta+\lambda_{\rm R}/2}{2(\mu-\lambda_{\rm R}/2)^2} - 2\Delta/\lambda_{\rm R}\frac{1}{\mu+\Delta}\right]\frac{\pi k_{\rm B}^2T}{12}. \quad (22)$$

Herein, $\theta(x)$ is the step function. Finally for the region (iv), I obtain

$$\sigma^s_{xy} = -\frac{\mu(\mu+\Delta)}{\mu^2-\lambda_{\rm R}^2/4}\frac{e}{4\pi}, \quad (23)$$

$$\alpha^s_{xy} = \frac{2\Delta(\mu^2+\lambda_{\rm R}^2/4)+\mu\lambda_{\rm R}^2}{(\mu^2-\lambda_{\rm R}^2/4)^2}\frac{\pi k_{\rm B}^2T}{24}. \quad (24)$$

All these expressions have taken into account the contributions from both Dirac points.

In Figs. 2 and 3, the zero-temperature SHC and the corresponding low-temperature SNC as functions of μ are shown for two special cases $\lambda_{\rm R}=0$ and $\Delta=0$, respectively. When $\lambda_{\rm R}=0$, the SHC and SNC are constant when the Fermi level is in an energy gap, and they disappear when $|\mu|\to\infty$. The SHC is symmetric with respect to the middle of the gap, while the SNC is antisymmetric (also see Eqs. (15) and (16)). When $\Delta=0$, the SHC and SNC are constant in the limit of $|\mu|\to\infty$. This can be also seen in Eqs. (19) and (22). The SHC is antisymmetric with respect to the change in the Fermi level sign, while the SNC is symmetric.

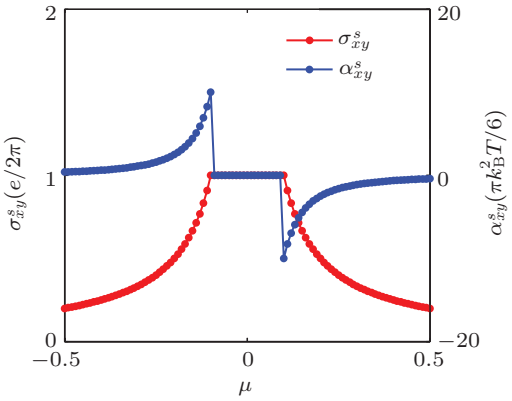


Fig. 2. (colour online) Spin Hall conductivity (dashed red curve) and the corresponding low-temperature spin Nernst conductivity (solid blue curve) for $\Delta=0.1$, and $\lambda_{\rm R}=0$.

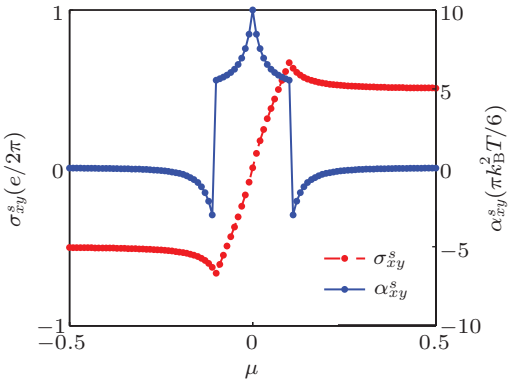


Fig. 3. (colour online) Spin Hall conductivity (dashed red curve) and the corresponding low-temperature spin Nernst conductivity (solid blue curve) for $\Delta=0$, and $\lambda_{\rm R}=0.1$.

When both intrinsic and Rashba spin–orbit interactions are present, we consider three cases:[19] $\lambda_{\rm R}>2\Delta$ (topological trivial phase), $\lambda_{\rm R}<2\Delta$ (topological phase), and $\lambda_{\rm R}=2\Delta$ (phase boundary). The dependence of zero-temperature SHC and low-temperature SNC on the chemical potential in the three cases are shown in Fig. 4 ($\Delta=0.1$ and $\lambda_{\rm R}=0.01$), Fig. 5 ($\Delta=0.1$ and $\lambda_{\rm R}=0.2$), and Fig. 6 ($\Delta=0.01$ and $\lambda_{\rm R}=0.2$), respectively. In the topological phase (see Fig. 4), the SHC and SNC are similar to those for $\lambda_{\rm R}=0$. In the gapped region $[-\Delta,\Delta-\lambda_{\rm R}]$ (region (iii)), the SHC and SNC are constant. However, there is a kink in the SHC in the region $[\Delta-\lambda_{\rm R},\Delta+\lambda_{\rm R}]$ (region (ii)). The corresponding SNC is discontinuous at the interface between regions (i) and (iii). The kink and discontinuity result from the splitting of the energy band induced by the Rashba spin–orbit interaction. On the phase boundary (see Fig. 5), the SHC and SNC are divergent at the threefold degenerate point $\mu=-\Delta$ (see Fig. 1(b)). In the topological trivial phase (see Fig. 6), the SHC and SNC are divergent at the degenerate point $\mu=-\Delta$, where the top of the

upper valence band touches the bottom of the lower conduction band (see Fig. 1(c)).

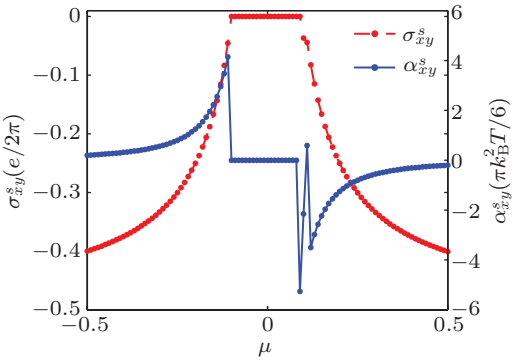


Fig. 4. (colour online) Spin Hall conductivity (dashed red curve) and the corresponding low-temperature spin Nernst conductivity (solid blue curve) for $\Delta = 0.1$, and $\lambda_R = 0.01$.

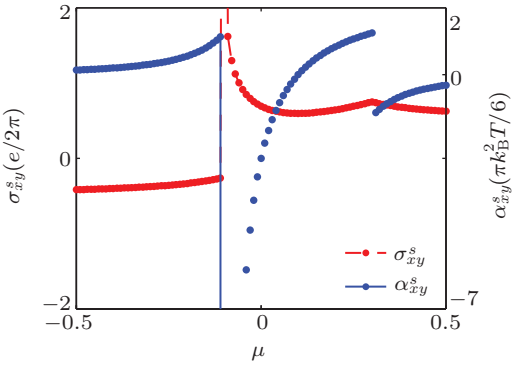


Fig. 5. (colour online) Spin Hall conductivity (dashed red curve) and the corresponding low-temperature spin Nernst conductivity (solid blue curve) for $\Delta = 0.1$, and $\lambda_R = 0.2$.

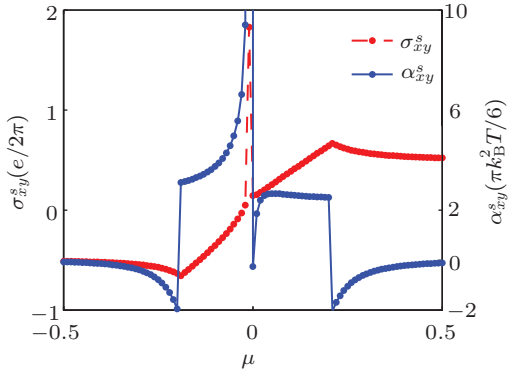


Fig. 6. (colour online) Spin Hall conductivity (dashed red curve) and the corresponding low-temperature spin Nernst conductivity (solid blue curve) for $\Delta = 0.01$, and $\lambda_R = 0.2$.

4. Discussion and conclusion

In summary, the SHC and SNC in the Kane–Mele model have been studied. The analytical expressions of the intrinsic contributions are obtained. The dependencies of zero-temperature SHC and low-temperature SNC on the chemical potential are analyzed. In the limit of the vanishing Rashba term and in the topological phase, the SHC is constant and the SNC is zero when the chemical potential is in the gap. However, there is a kink in the conductance in the topological phase. The kink is associated with the splitting of the energy band induced by the Rashba spin–orbit interaction. On the phase boundary, the kink becomes a divergent point at the position where the top of the upper valence band touches the bottom of the lower conduction band. In the topological trivial phase, the divergence becomes more pronounced with an increasing Rashba spin–orbit interaction.

References

[1] Hirsch J E 1999 *Phys. Rev. Lett.* **83** 1834
[2] Murakami S, Nagaosa N and Zhang S C 2003 *Science* **301** 1348
[3] Sinova J, Culcer D, Niu Q, Sinitsyn N A, Jungwirth T and MacDonald A H 2004 *Phys. Rev. Lett.* **92** 126603
[4] Kato Y K, Myers R C, Gossard A C and Awschalom D D 2004 *Science* **306** 1910
[5] Kimura T and Otani Y 2007 *Phys. Rev. Lett.* **99** 196604
[6] Brüne C, Roth A, Novik E G, König M, Buhmann H, Hankiewicz E M, Hanke W, Sinova J and Molenkamp L W 2010 *Nature Phys.* **6** 448
[7] Berry M V 1984 *Proc. R. Soc. London Ser.* B **392** 45
[8] Sundaram G and Niu Q 1999 *Phys. Rev.* B **59** 14915
[9] Uchida K, Takahashi S, Harii K, Ieda J, Koshibae W, Ando K, Meakawa S and Saitoh E 2008 *Nature* **455** 778
[10] Jaworski C M, Yang J, Mack S, Awschalom D D, Heremans J P and Myers R C 2010 *Nature Mater.* **9** 898
[11] Xiao D, Yao Y, Fang Z and Niu Q 2006 *Phys. Rev. Lett.* **97** 026603
[12] Novoselov K S, Geim A K, Morozov S V, Jiang D, Zhang Y, Dubonos S V, Grigorieva I V and Firsov A A 2004 *Science* **306** 666
[13] Kane C L and Mele E J 2005 *Phys. Rev. Lett.* **95** 146802
[14] Kane C L and Mele E J 2005 *Phys. Rev. Lett.* **95** 226801
[15] Dedkov Y S, Fonin M, Rüdiger U and Laubscha C 2008 *Phys. Rev. Lett.* **100** 107602
[16] Varykhalov A, Sánchez-Barriga J, Shikin A M, Biswas C, Vescovo E, Rybkin A, Marchenko D and Rader O 2008 *Phys. Rev. Lett.* **101** 157601
[17] Castro Neto A H and Guinea F 2009 *Phys. Rev. Lett.* **103** 026804
[18] Imura K, Kuramoto Y and Nomura K 2009 *Phys. Rev.* B **80** 085119
[19] Yamakage A, Imura K, Cayssol J and Kuramoto Y 2011 *Phys. Rev.* B **83** 125401
[20] Onoda S, Sugimoto N and Nagaosa N 2006 *Phys. Rev. Lett.* **97** 126602
[21] Onoda S, Sugimoto N and Nagaosa N 2008 *Phys. Rev.* B **77** 165103
[22] Kovalev A A, Tserkovnyak Y, Vyborny K and Sinova J 2009 *Phys. Rev.* B **79** 195129
[23] Kovalev A A, Sinova J and Tserkovnyak Y 2010 *Phys. Rev. Lett.* **105** 036601
[24] Smrčka L and Středa P 1977 *J. Phys.* C **10** 2153
[25] Dyrdał A, Dugaev V K and Barnaś J 2009 *Phys. Rev.* B **80** 155444